1981ApJ...246..515S

THE ASTROPHYSICAL JOURNAL, 246:515–525, 1981 June 1
© 1981. The American Astronomical Society. All rights reserved. Printed in U.S.A.

RAYLEIGH-TAYLOR OVERTURN IN SUPERNOVA CORE COLLAPSE

LARRY SMARR[1]
Department of Astronomy, University of Illinois
AND
JAMES R. WILSON, ROBERT T. BARTON, AND RICHARD L. BOWERS
Lawrence Livermore Laboratory
Received 1980 June 18; accepted 1980 December 9

ABSTRACT

We perform a two dimensional radiation diffusion coupled to hydrodynamics calculation of nonspherical instabilities in the collapsed core from a massive star. The core properties are taken from a one dimensional collapse calculated with detailed microphysics and neutrino transport. The shocked outer core [$0.7\ M_\odot \lesssim M(r) \lesssim 1.3\ M_\odot$] is found to contain three subregions. The innermost is doubly diffusive ("neutron fingers") unstable, the center subregion is dynamically unstable, and the outermost is stable. We find that the unstable part of the outer core overturns in ~ 5 ms without disturbing the inner unshocked core of $M \lesssim 0.7\ M_\odot$. This overturned outer core expands as a piston, creating an outgoing shock wave which may help power envelope ejection. This outer core overturn would seem to be a generic feature of core collapse which has heretofore been neglected.

Subject headings: hydrodynamics — shock waves — stars: interiors — stars: supernovae

I. INTRODUCTION

The question of whether neutrinos are decisive in causing envelope ejection following core collapse has had many answers since Colgate and White's (1966) original model of energy deposition. The discussion of this question was recently revived by Colgate and Petschek's (1979) suggestion that perhaps large scale core overturn can occur, driven by the lepton number inversion discussed earlier by Epstein (1979). A spherical supernova code with such an overturn mocked up (Bruenn, Buchler, and Livio 1979) showed that in the most optimistic case such a drastic core overturn could power the supernova ejection. Most recently Livio, Buchler, and Colgate (1979) have performed a two dimensional simulation of such an overturn. Unfortunately, their initial model corresponds to a higher adiabat than we used. We used the recent detailed precollapse evolutionary calculations of Weaver, Zimmerman, and Woosley (1978). Their calculation does not determine whether such core overturn would in fact occur in these lower entropy models.

Stimulated by Colgate's idea, we have begun a study of such nonspherical effects during core collapse. We have performed a two dimensional radiation diffusion coupled to hydrodynamics calculation on a core whose properties are taken from a more realistic one dimensional model with detailed microphysics and neutrino transport. We find that the outer shocked core [$0.7 < M(r)/M_\odot < 1.3$] does overturn in a few ms as suggested by Colgate *et al.* However, the inner unshocked core [$M(r) < 0.7\ M_\odot$] is isolated from this dynamics by the large gradient of density and discontinuity in entropy at the outer face of the inner core induced by the initial shock. The initial overturn of the outer core, which occurs on a time scale of 5 ms, is violent, but not violent enough to cause an explosion. Furthermore, we find that the overturn of the entire core on a time scale of 20–40 ms after bounce predicted by the above authors will not occur unless the substantial entropy gradient produced by the shock can be radiated away. Whether or not this can be accomplished is doubtful. The overturned outer core expands like a piston, creating an outgoing shock wave. We discuss whether this shock is energetic enough to power the supernova and whether the later neutrino cooling will eventually cause core overturn.

[1] Alfred P. Sloan Fellow.

II. THE ONE DIMENSIONAL MODEL

a) *Core Properties*

Using a spherical supernova code described elsewhere (Wilson 1979), we calculated an iron core collapse (from an initial $1.5\ M_\odot$ model supplied by Weaver and Woosley [private communication] and described in Weaver, Zimmerman, and Woosley 1978). The time to core bounce was ~ 250 ms. At bounce an outgoing shock forms at $M(r) \approx 0.7\ M_\odot$, but after moving out to about $1\ M_\odot$ it becomes a standing accretion shock. Within another 20 ms the entire $1.4\ M_\odot$ core has fallen through the shock and a steady state core is reached. Other changes to the core, such as core neutronization and neutrino losses, will take place on a much longer time scale ($\gtrsim 100$ ms). Therefore, at this time, $t_{on} = t_{bounce} + 20$ ms, we study the core for nonspherical instability.

Before we discuss the two dimensional model, we review the physics of the core at $t = t_{on}$. This review is useful for two reasons. First, it will select out the key physical features from the one dimensional (1D) calculation which we believe to be model independent. Second,

© American Astronomical Society • Provided by the NASA Astrophysics Data System

1981ApJ...246..515S

we will study the spatial relationships between these key quantities that determine where and if instability occurs.

We give schematic diagrams of the core profiles in Figure 1. This figure plots against mass of the inner 1.6 $M_\odot$ the following four quantities: (*a*) the entropy per baryon S, (*b*) the number of leptons per baryon Y_l, (*c*) the mass fraction of heavy nuclei X_A, (*d*) the adiabatic index γ, and (*e*) a measure of the local instability (see eq. [3] below). Each part of the figure contains a profile at the onset of core collapse ($t = 0$), adapted from Weaver and Woosley (private communication), and at 20 ms after bounce ($t = t_{on}$).

The core has been divided into an inner core [$M(r) < 0.7\ M_\odot$] denoted region I, an outer core [$0.7\ M_\odot < M(r) < 1.3\ M_\odot$] containing regions II, III, and IV, and a mantle [$M(r) > 1.3\ M_\odot$]. The existence of an inner core region I is generic to iron core collapse (Wilson 1979). It contains the matter whose infall was homologous and which bounced as a unit. It is therefore unshocked. The boundary between regions I and II represents the point at which the shock first formed, and the outer boundary of region IV represents the shock position at time t_{on}. The outer boundary of region IV also represents the neutrinosphere, the radius where neutrinos decouple from the matter. The material in regions II–IV has therefore been shocked. The reason for subdividing the outer core into the three regions shown is dictated by the stability conditions to be discussed below. We note that the shock has become an accretion shock by $t = t_{on}$ and is located essentially at the neutrinosphere.

We now review the physical processes which determined the shape of the profiles at time t_{on} (Fig. 1). The uniform rise in core entropy per baryon from 1 to ~ 2 is due primarily to neutrino bulk viscosity; there has been no shock heating in region I. The entropy per baryon in the outer core increases initially to about 5 as the shock sweeps outward. However, it quickly begins to decrease because of neutrino cooling. This decrease in S is greater near the interface I–II than near the outside since region II has had more time to cool than regions III and IV. About 85% of the energy is carried off by muon and tau neutrinos which are pair-produced at the high temperatures (> 7 MeV) reached behind the shock. We note that S is relatively flat in the central portion of region III. The entropy of the shock is close to its initial ($t = 0$) value.

The total lepton number Y_l shown in Figure 1*b* is defined by

$$Y_l = (n_e + n_\nu)/n_b\ , \qquad (1)$$

where n_e is the total electron number density, n_ν is the electron neutrino number density, and n_b is the baryon number density (free plus bound in nuclei). The negative Y_l gradient in the outer part of region I results from the high neutrino emission rate of the matter just prior to bounce, and the fact that the closer the matter is to the I–II interface the more time it has had to emit. The discontinuity in Y_l across the interface results from the discontinuous drop in density across the shock formed at bounce. This drop forces n_e and n_b to be discontinuous, while neutrino diffusion tends to maintain a smooth variation in n_ν across the shock. From equation (1) this implies that Y_l is discontinuous. The arguments used above to explain the outward decrease in Y_l in the inner core also apply to its continued decrease through regions II and III. The matter in the outer core consists mainly of free nucleons, while the matter ahead of the shock contains heavy nuclei (Fig. 1c). Electron capture can occur on all free nucleons, but it is limited to a few loosely bound ones in the heavy nuclei. This results in the rapid increase in Y_l across the outer core-mantle interface.

The mass fraction of heavy nuclei X_A is shown in Figure 1*c*. At bounce the inner core matter undergoes partial thermal decomposition to He. The matter in the outer core is shock decomposed to free nucleons. Outside the shock X_A rapidly approaches its initial value $X_A = 1$.

Figure 1*d* shows the adiabatic index γ of the gas from our equation of state:

$$P = (\gamma - 1)\rho\epsilon\ , \qquad (2)$$

where ρ is the matter density and ϵ is the specific energy per gram. In the inner core, the principal species contrib-

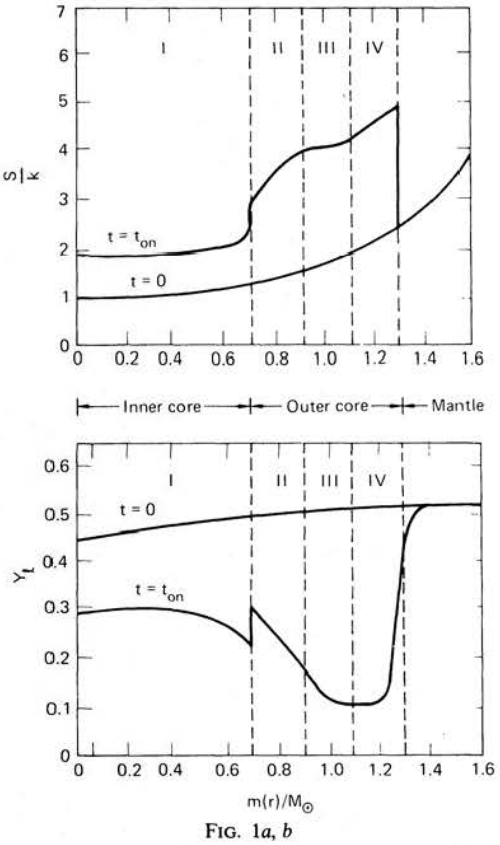


FIG. 1*a*, *b*

FIG. 1.—Profiles of (*a*) (*top*) entropy per baryon s/k; (*b*) (*bottom*) ratio of lepton to baryon number density Y_l; (*c*) (*top*) mass fraction of heavy nuclei X_A; (*d*) (*bottom*) adiabatic index γ (see eq. [2]) as adapted from the one dimensional calculation, and (*e*) a local measure of instability against convection (see eq. [3]). Shown are values at $t = 0$ (onset of collapse) and $t = t_{on}$ (beginning of two dimensional model). The inner and outer core have been divided into regions I–IV based on stability criteria discussed in the text. At $t = t_{on}$ the shock and neutrinosphere are located at the outer core-mantle interface.

© American Astronomical Society • Provided by the NASA Astrophysics Data System

1981ApJ...246..515S

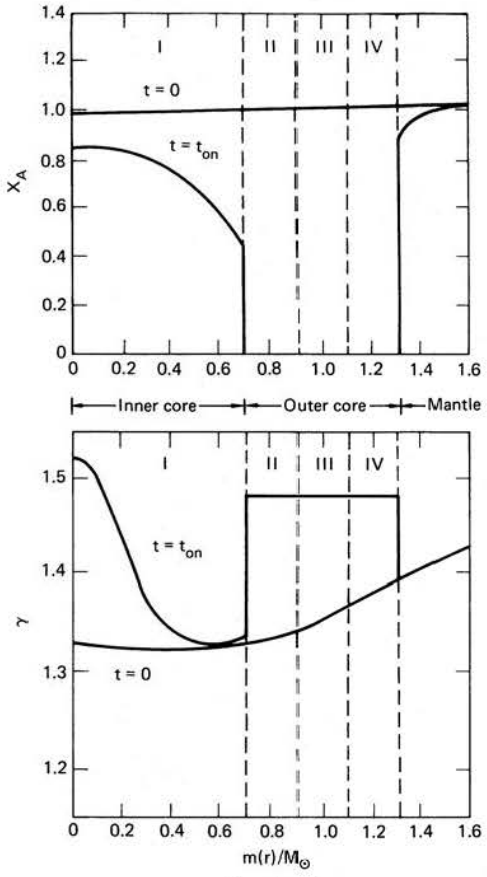


FIG. 1c, d

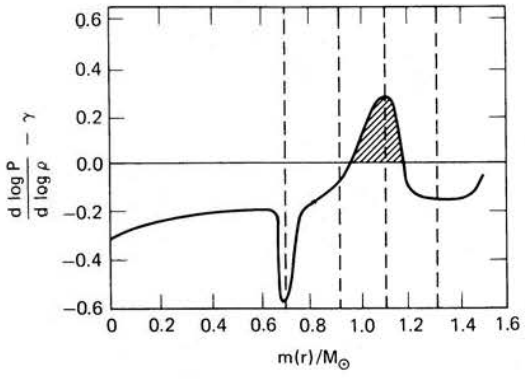


FIG. 1e

uting to γ varies smoothly from about 1.56 to 1.33. The dominant species in the shocked matter of the outer core are (1) the hot nonrelativistic nuclear gas and (2) the relativistic electron gas, giving an effective $\bar{\gamma} = \partial \log p/\partial \log \rho = 1.45$. In the shocked region, a large fraction of the material energy is tied up in the decomposition energy of Fe. Using the definition of adiabatic index in equation (2) then yields: $\gamma = 1.34$. For the two dimensional (2D) calculation in which we could only use a spatially constant γ in each region, we chose $\gamma = 1.40$ as an average value. Ahead of the shock γ reverts nearly to its initial value for hot nuclei and electrons.

Figure 1*e* shows the quantity $d \ln P/d \ln \rho - \gamma$ which is proportional to the negative of A (eq. [3]). Negative values correspond to stability against convection. The sharp decrease at the I–II interface reflects the stabilizing effect of the entropy jump formed at bounce. The only unstable region (shown crosshatched) occurs across the II–IV interface.

b) Core Stability

As discussed by Livio, Buchler, and Colgate (1979, hereafter LBC), we can use the standard linear stability theory to determine which regions are subject to instability. The instability test is whether

$$A = \frac{1}{\rho}\left(\frac{d\rho}{dr} - \frac{1}{c_s^2}\frac{dP}{dr}\right) = -\frac{1}{\rho c_s^2}\left[\left(\frac{\partial P}{\partial S}\right)_{\rho, Y_l}\frac{ds}{dr} + \left(\frac{\partial P}{\partial Y}\right)_{\rho, S}\frac{dY_l}{dr}\right] \quad (3)$$

is anywhere positive (LBC, eq. [1]), where c_s is the local adiabatic speed of sound. We use equation (3) to investigate the instability of the core region by region.

In contrast to LBC, who used the equation of state (EOS) of Bruenn (1975) and whose initial core model correspond to a relatively high adiabat, we use a more recent EOS which is similar to the EOS described by Lamb *et al.* (1978) and a low entropy initial core. This is a crucial difference, since with the LBC initial model the core undergoes a thermal bounce at low density, while with the current model, core bounce occurs at nuclear density. As we see below, the difference in thermodynamic core structure determines the difference in stability.

From equation (3) we see that since the two partial derivatives are usually positive, the positive slopes in S and Y_l stabilize. Turning to Figure 1, we consider the four regions of the core:

Region I.—Although Y_l is slightly unstable in the outer part of the inner core, the sharp decline in X_A compensates by causing S to rise slightly. This region should be nearly stable.

Region II.—The interface between the inner core (I) and the outer core (II, III, IV) is strongly stabilized by the discontinuous positive jumps in S and Y_l. We therefore expect that any motion in the outer core will be isolated stably from the inner core. In region II, Y_l is unstable while S is stable. Since S is changing by heat flow carried by μ and τ neutrinos at a rate ~ 10 times faster than Y_l is changing by leptonic flow carred by e neutrinos, this region should be a doubly diffusive unstable region (Turner 1974). It will destabilize on a thermal diffusion time scale.

Region III.—Here S is neutrally stable and Y_l is unstable. This is the most unstable region. It should destabilize on a dynamic time scale.

Region IV.—This region is strongly stabilized by positive gradients in both S and Y_l.

© American Astronomical Society • Provided by the NASA Astrophysics Data System

1981ApJ...246..515S

Mantle.—The interface is, strictly speaking, unstable because of the drastic drop in S. However, this shock front is also the neutrinosphere at this time, and thus a simple stability analysis is inappropriate here. In this paper we will not be concerned with this interface or the rest of the envelope.

Thus there are two unstable regions (II, III), but the nature of the instability is complicated by the presence of two types of gradients (S, Y_l). In order to make clear the subsequent calculation, we briefly review convective instabilities.

The usual form of turbulent convection (Spiegel 1971, 1972) we term microconvection, indicating that the size of individual convective cells or bubbles is very small compared to the size of the convection zone. That such microconvection should occur in collapsed cores driven by the lepton inversion was first pointed out by Epstein (1978). Subsequently both Wilson and Arnett added microconvective routines to their collapse codes. These routines were modeled on standard mixing length algorithms used in stellar evolution codes. Indeed, such a routine was used in the one dimensional calculation discussed above. There is no dramatic difference in the core evolution when the microconvection is used. This is because microconvection mixes locally, not globally, on a long ($\sim 10^2$ ms) time scale. We may think of microconvection as a higher L number (angular) and high K number (radial) perturbation. There is some question whether this small scale convection can actually take place in the face of neutrino viscosity (Kazanas and Schramm 1979). A rough estimate of the Reynolds number of the neutrino trapped outer core yields 10^3–10^4, high enough to smooth out many small scale fluctuations.

The other extreme to microconvection is macroconvection, in which a large scale overturn of the entire unstable region takes place. The possibility that the whole core could so overturn was suggested by Colgate and Petschek (1979). Their point was that in a region such as III, the bouyant instability can be modeled as a Rayleigh-Taylor instability, where a light fluid (high Y_l) is accelerating a heavy fluid (low Y_l). We agree with this idea, but differ in our analysis of which regions of the core are susceptible to this instability. From our work, it would appear that only region III, and not the entire core, is dynamically unstable on the time scale of $\sim$ 5–30 ms after bounce as discussed by Bruenn, Buchler, and Livio (1979) and Livio, Buchler, and Colgate (1979).

Region II has two opposing stability gradients with different diffusion time scales. The most well known example of doubly diffusive convection (see, e.g., Turner 1974) are salt fingers. Here hot salty water overlies cold fresh water. If a perturbation in the interface is made, the heat diffuses faster than the salt, leaving dynamically growing "salt fingers." Just so here, the heat diffuses by *pair*-produced e, μ, and τ neutrinos (zero net change of lepton number) about 10 times faster than lepton number diffuses by the difference of ν_e and $\bar{\nu}_e$ currents. Since the heavy material here is mainly neutrons, we call this effect "neutron fingers." Normally, the fastest diffusion (temperature) time scale is slow compared to the hydrodynamic (free fall) time scale. However, in the one dimensional core collapse, we find these time scales comparable, of the order of a few milliseconds. This is because the luminosity in neutrinos is about 5×10^{53} ergs s^{-1}, comparable to the gravitational energy release from exchanging regions II and III in $\sim$ 5 ms. Thus, if we employ radiation diffusion in our two dimensional model, we expect regions II and III to be equally unstable.

III. THE TWO DIMENSIONAL MODEL

a) Initial Core Configuration

In order to calculate an axisymmetric hydrodynamic core in a reasonable amount of computer time, the detailed microphysics must be greatly simplified over the spherical code. We have done this in a way which we think retains the key features of the problem. Our code is Eulerian with the capability of following separate fluids. We therefore set up a 2D core with four fluids corresponding to regions I–IV of Figure 1. These fluids are allowed to communicate thermally if the radiation diffusion equation (discussed below) is turned on, but they stay "chemically separate." That is, each zone of the finite difference grid records the volume fraction of the zone occupied by each of the four fluids and uses these volume fractions to construct partial pressures, transport terms, etc. We believe this is physically appropriate since "chemical mixing" requires transport of lepton number which occurs on a timescale long compared to the dynamical time scale.

The central density is set to 3×10^{14} g cm^{-3} and the central pressure to 9.24×10^{33} dyn cm^{-2}, as suggested by the one dimensional model at $t = t_{on}$. In each region the equation of state of the initial core is:

$$P = K_i \rho^{\gamma_i}, \quad i = \text{II, III, IV}, \tag{4}$$

where K_i and γ_i can be chosen separately for each region. The density in region I exceeds nuclear density, so a term representing the nuclear hardening of the EOS is added:

$$P = 5.8 \times 10^4 \rho^2 + K_1 \rho^{\gamma_1}, \quad i = \text{I}. \tag{5}$$

Using Figure 1*d* as a guide, we chose $\gamma_1 = \frac{4}{3}$ and $\gamma_{II} = \gamma_{III} = \gamma_{II} = \frac{7}{5}$. In retrospect we could have used a higher γ (nearer 1.5) for the three outer regions, but we do not believe this is essential. K_i's are chosen by integrating the equation of hydrostatic equilibrium from the center outward, to find the density profile given an appropriate choice for K_1 (see Table I). When a region boundary is reached, a jump in ρ is specified across the boundary, which fixes K_i in the next zone. Physically, this means we specify separate adiabats for each region such that the total system is in hydrostatic equilibrium initially.

The choice of the density jumps is motivated by the instability analysis of § II*b* above. Ideally, we would use a code that calculated the hydrodynamic (ρ), thermal (S), and chemical (Y_l) properties of each point of the core. Such a calculation is possible, but would require a much larger effort than the problem calls for at this stage. Therefore, we have tried to simulate the buoyancy instability of the Y_l inversion in region III by a density inversion

© American Astronomical Society • Provided by the NASA Astrophysics Data System

1981ApJ...246..515S

TABLE 1

A. Pure Hydrodynamic Run

Region	$K_i/10^{14}$	γ	ρ_+/ρ_-
I	2.00	1.33	...
I/II	...	...	0.32
II	1.77	1.40	...
II/III	...	...	2.05
III	0.65	1.40	...
III/IV	...	...	0.49
IV	1.77	1.40	...

B. Radiation Hydrodynamic Run

Region	$K_i/10^{14}$	$C_{v_i}/10^{15}$	γ	ρ_+/ρ_-	T_+/T_-
I	2.00	2.5	1.33	...	...
I/II	...	...	...	0.25	3.24
II	1.71	2.5	1.40	...	...
II/III	...	...	...	1.28	2.01
III	1.34	1.56	1.40	...	...
III/IV	...	...	...	0.78	0.45
IV	1.71	2.5	1.40	...	...

which yields a buoyancy force of roughly the same magnitude. To estimate the density jump, we assume that it will be approximately equal to the drop in Y_l from region II to region III, i.e., between ~ 1.4 and 1.7. We base this guess on the perfect gas law which, for constant temperature, would say the same pressure change occurs for a jump ρ_1/ρ_2 as for a mean molecular weight drop of μ_1/μ_2. Future work is required to make sure our procedure does not affect the physical outcome of the instability.

Using the above method, we ran a number of pure hydrodynamic calculations discussed in the next section. However, such calculations ignore the doubly diffusive "neutron finger" instability of region II. Therefore we added a radiation diffusion program which stimulates the heat conduction of the pair neutrinos. The heat flow in the 2D calculation was made equal to the heat flow in the 1D code by selecting the opacity in each region for the 2D code such that with the temperatures present initially the heat flow as a function of radius was approximately the same as in the 1D calculation. For these later runs we use an equation of state:

$$P = (\gamma - 1)\rho\epsilon \ , \quad \epsilon = C_v T \ , \tag{6}$$

and use the radiation diffusion equation to determine T and thus ϵ (in addition to the usual PdV term). To set up the initial T field we specify C_{v_i} separately in each zone. Table 1 lists the values chosen along with the equivalent K_i's. Note equation (6) reduces to equation (4) in the adiabatic (pure hydrodynamic) case by:

$$T = \frac{K_i \rho^{\gamma - 1}}{C_v(\gamma - 1)} \ . \tag{7}$$

For the radiation diffusion runs we chose C_v the same in regions I, II, and IV, but lower by 1.6 in region III. This simulates the fact that leptons are less numerous in that region. To get 1.6 one has to consider the free baryons in region III contribute from one-third to one-half of the pressure, which moderates the effect of the drop in Y_l.

Because ρ and T are adiabatically related by equations (6)–(7), the entropy throughout each region is constant, and the distributed instabilities inherent in the 1D model have been replaced by instabilities across the II–III boundary. The 2D calculation exhibits the global response to these instabilities. However, we emphasize that the character of these instabilities were dictated by distributed instabilities inherent in the ID model.

b) Large Density Inversion

To try to maximize the instability growth rate we first ran a series of three pure hydrodynamic runs with a larger jump in $\rho_{II}/\rho_{III} = 2.05$ than we thought was justified by our 1D stability analysis. The resulting profile of $\log \rho$ is shown in Figure 2. The three runs were to test the dependence on the angular mode of the initial perturbation. We used perturbations with angular symmetries of 90°, 45°, and 22°.5. By using a density inversion we have replaced the actual chemical inversion (Y_l) instability by a true Rayleigh-Taylor (RT) instability. This follows the spirit of Colgate and Petschek's (1979) original suggestion. The RT instability starts off in the small amplitude limit by exponentially growing as $e^{t/\tau}$ with time constant τ given by

$$\tau = (Ag2\pi/\lambda)^{1/2} \ ,$$

where $A = (\rho_2 - \rho_1)/(\rho_2 + \rho_1)$, g is the local acceleration, and λ is the wavelength of the perturbation on the surface. We use this only as an estimate to check our code results, since it is derived (see, e.g., Chandrasekhar 1961) for slab geometry with constant-density incompressible flow. For the 90° run we have

$$A = (\rho_2/\rho_1 - 1)/(\rho_2/\rho_1 + 1) = 0.34 \ ,$$

$g = GM_\odot/(2.4 \times 10^6 \text{ cm})^2 = 2.3 \times 10^{13}$ cm s^{-2}, $\lambda = \pi(2.4 \times 10^6 \text{ cm}) = 7.5 \times 10^6$ cm, yielding $\tau_{90} = 0.4$ ms. For the other two runs, $\tau_{45} = 0.55$ ms and $\tau_{22} =$

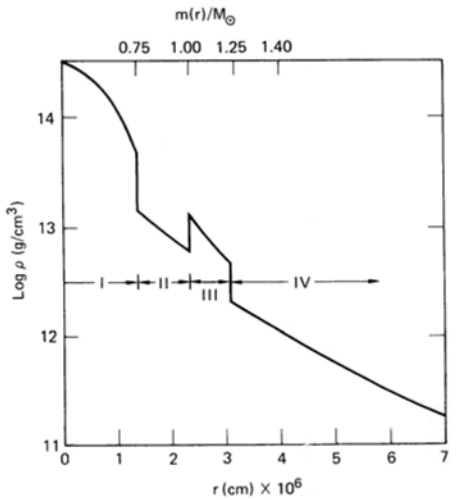


FIG. 2.—Density vs. interior mass fraction adapted for the two dimensional pure hydrodynamic calculations. Also shown are the stability regions defined in the one dimensional mode.

© American Astronomical Society • Provided by the NASA Astrophysics Data System

1981ApJ...246..515S

0.54 ms. (Note our 22°.5 run had slightly different radii for the boundaries between the regions.)

The actual form of the density perturbation used was

$$\rho = \rho_0[1 \pm \epsilon(B_n - \cos^2 n\theta)], \quad (9)$$

$$B_n = \tfrac{1}{2}\{1 - (1 + \mu)/[(1 - \mu)(4n^2 - 1)]\}, \quad (10)$$

where $\mu = \cos(\pi/2n)$ and $n = 1, 2, 4, \ldots$ for 90°, 45°, 22°.5, ... This gives $B_n = \frac{1}{3}$ for each n. Our runs used an $\epsilon = 10^{-3}$ so that the maximum perturbation had amplitude 6.6×10^{-4}. The perturbation was set on the boundary of regions II/III and linearly extended upward and outward to the next boundary, where the perturbation vanishes, with the plus sign used in region II and the minus sign used in region III. We would estimate that for this perturbation to exponentiate up to finite amplitude $[(0.1\text{–}0.5)\rho_0]$ requires 5 to 6 e-foldings or 2.5–3.0 ms after the start of the calculation.

The results of the calculation with 90° are shown in Figures 3*a*–3*e*. Actually, we show only the inner one-

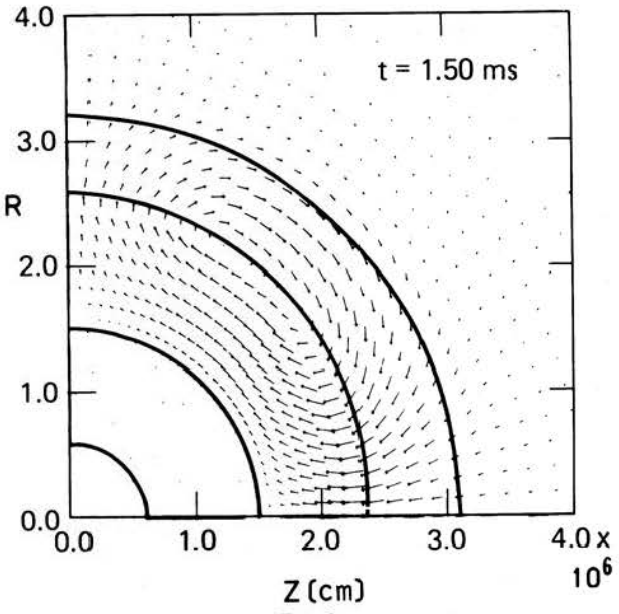


FIG. 3*a*

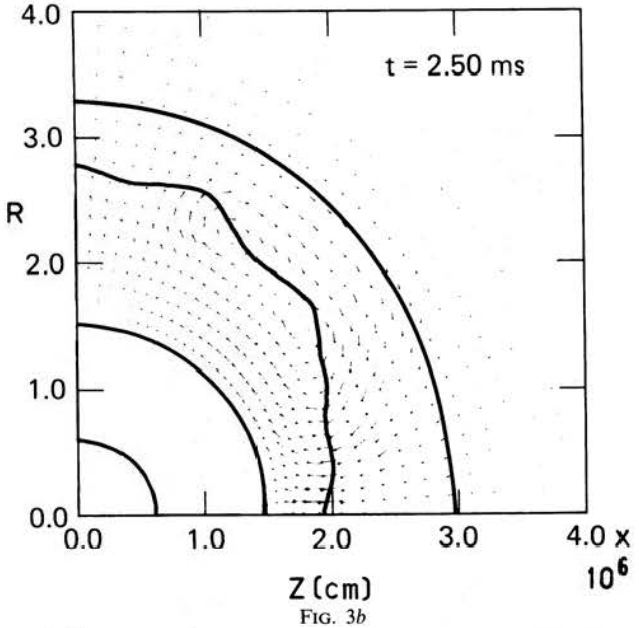


FIG. 3*b*

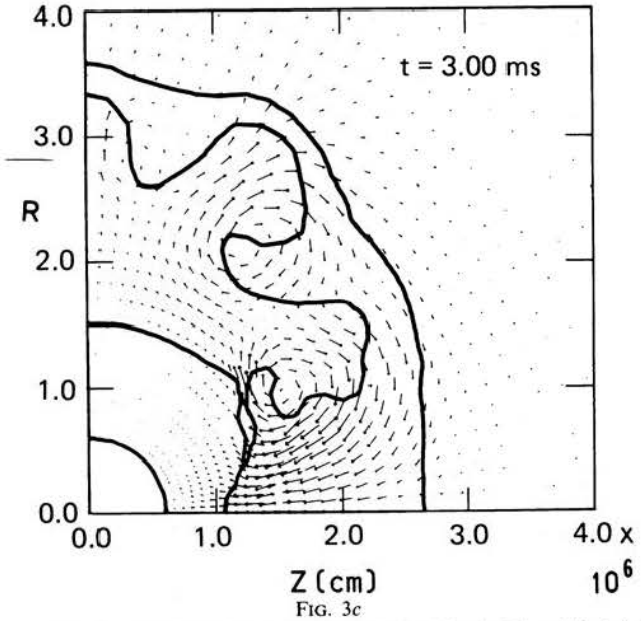


FIG. 3*c*

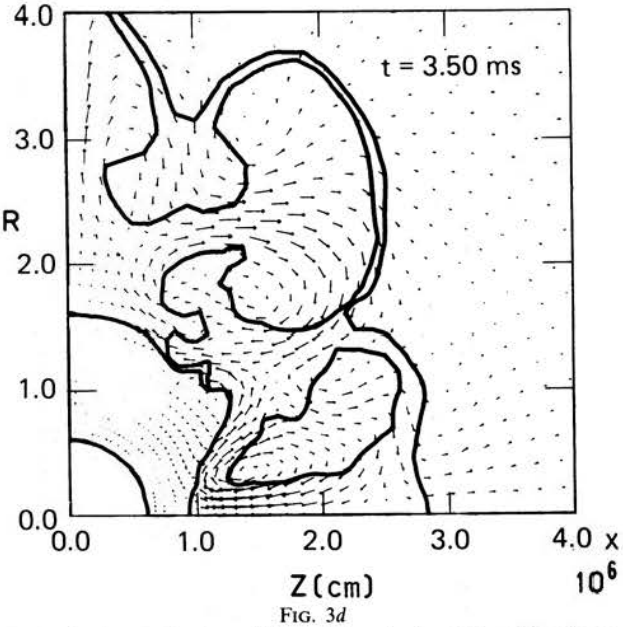


FIG. 3*d*

FIG. 3.—Motion of the fluid regions obtained for the 90° model. Only the inner portion is actually shown. The central region ($r < 0.6 \times 10^6$ cm) was excluded from the calculation. Boundaries separate material according to its initial density distribution (Fig. 2). The time between each frame is 0.5 ms, with the first (3*a*) 2 ms into the evolution. Arrows represent local fluid velocity with length proportional to speed. The maximum values shown are (*a*) 4.2×10^8 cm s^{-1}, (*b*) 1.85 × 19^9 cm s^{-1}, (*c*) 4.06×10^9 cm s^{-1}, (*d*) 5.27×10^9 cm s^{-1}, (*e*) 4.9×10^9 cm s^{-1}, and are comparable to the local sound speed.

© American Astronomical Society • Provided by the NASA Astrophysics Data System

1981ApJ...246..515S

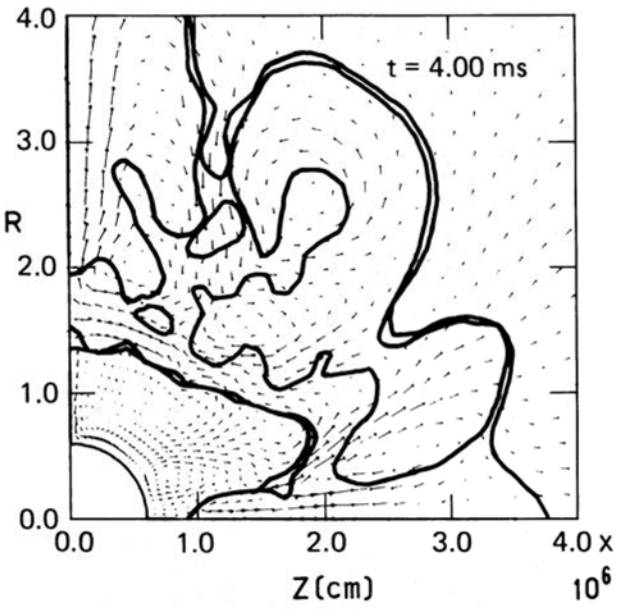


FIG. 3e

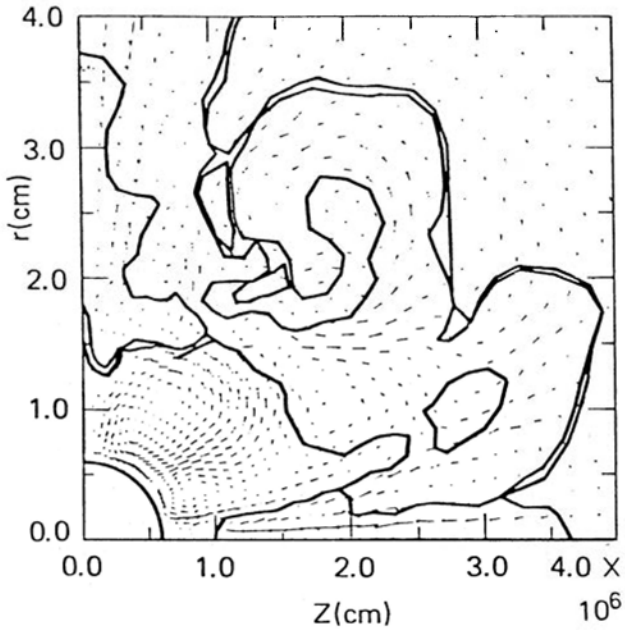


FIG. 3f

fourth of the radius. That is, the grid extends out to 17×10^6 cm, but we view a closeup of the inner 4×10^6 cm in Figure 3. The total grid has 60 radial zones and 30 angular zones. There are roughly 300 time cycles per millisecond of physical time. The vectors in Figure 3 represent the direction and magnitude of the fluid velocity at each point on the grid. Each frame (*a*)–(*e*) is separated by 0.5 ms and has a different scale for vector length. The interfaces between the fluids from the four original regions are indicated. The innermost 0.1 $M_\odot$ ($r < 0.6 \times 10^6$ cm) of the fluid is not evolved because the fine angular zoning would limit the time steps unnecessarily.

As Lamb (1945) points out on p. 371, the effect of perturbing the discontinuous interface surface is to make it a vortex sheet. Thus, as the perturbation exponentiates in amplitude, the velocity assumes the vortex pattern seen in Figure 3*a*. Even though the velocities are fairly large by $t = 2$ ms, there has not been time enough for matter to move very far, as indicated by the near sphericity of the interfaces. Note that the "$L = 2$"-like vortex results from the angular dependence of the initial perturbation.

By 2.5 ms (Fig. 3*b*), the perturbation has reached finite amplitude, exactly matching our estimated time above. However, a rather unexpected thing happens in that the large "$L = 2$" vortex breaks into two "$L = 4$" vortices. These two vortices dominate the rest of the calculation. By 3 ms (Fig. 3*c*), the characteristic "spike and bubble" nonlinear regime is reached. The horizontal "foot" on the spike is caused by a Kelvin-Helmholtz (KH) instability as the spike shears by the bubble. In Figure 3*d*, $t = 3.5$ ms, the fully developed mushroom bubble is present. The mushroom shape results from a KH vortex instability on each descending spike bordering the bubble. Note that such vortices are on the lower bubble as well, but that its neck has been severed by the flow. By 4.0 ms (Fig. 3*e*), the inversion of regions II and III is complete.

We note that while large surface oscillations are induced on the inner core (region I), it does not go unstable. We carried out the calculation until 4.6 ms and the core simply sloshes around stably. Figure 3*f*, at 4.5 ms, does show that this sloshing induces large scale vortices in region I which extend down to our inert core. Thus, for the large density inversion, region I is convectively mixed, but region I does not mix with region II. We will see that for the more realistic small density inversion these large vortices are not induced in region I. Thus, on the time scale we find outer core overturn but not total core overturn. We should remark that because we demand axisymmetry, the bubbles and spikes are actually toroidal; that is, one must rotate Figure 3 around the horizontal symmetry axis to get the full three dimensional picture. In reality, if axisymmetry were not demanded, the toroidal spikes and bubbles might break up into quasi-spherical blobs.

Some of these nonlinear RT and KH instability stages have been studied before. Harlow and Welch (1966), Daly (1967), and Crowley (1970) performed numerical calculations of incompressible fluids in slab geometry leading up to the "foot" formation. Ratafia (1973) was able experimentally to photograph the development of the nonlinear instability of water on alcohol. His Figure 3 shows an amazingly close similarity to our Figure 3*a*–*d*, even though the densities of the fluids in his experiment are 10^{-12} the densities in our collapsed stellar core.

Since our calculation indicates that the "$L = 4$" mode is preferred, we performed a 45° calculation, with perturbation given by $n = 2$ in equations (9) and (10). A very similar development of spike and bubbles, foot formation, and layer inversion occurred on roughly the same time scale (see Figs. 4*a*, 4*b*). However, there was no

© American Astronomical Society • Provided by the NASA Astrophysics Data System

1981ApJ...246..515S

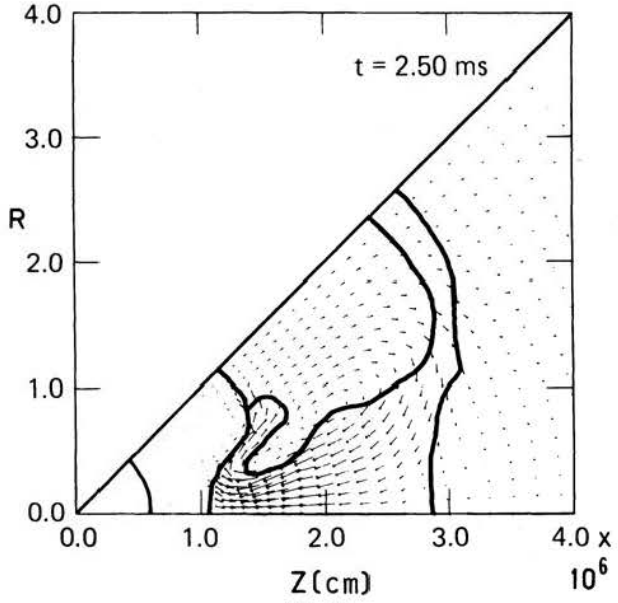


FIG. 4*a*

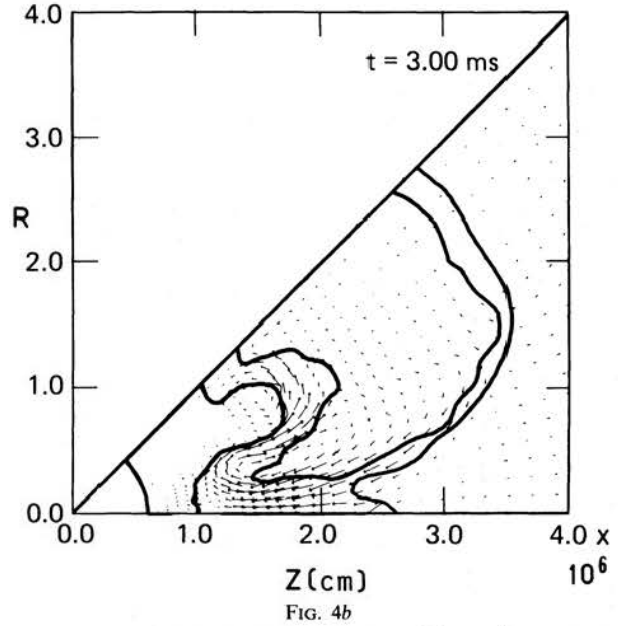


FIG. 4*b*

FIG. 4.—Fluid motion for the 45° problem. (*a*) inner $\frac{1}{4}$ of the mesh shown at 2.5 ms into evolution. The maximum velocity has magnitude 5.24×10^9 cm s^{-1} at this time. (*b*) The inner 1.4 of the problem 3.0 ms into evolution. The maximum speed is 8.09×10^8 cm s^{-1}. (*c*) The entire grid 4.87 ms into the evolution. Note the shock wave at a radius of approximately 1.3×10^7 cm. The peak velocity behind this outward going shock is 2.1×10^9 cm s^{-1}.

indication that the "$L = 4$" mode wanted to break up into "$L = 8$." The inner core behaved in the same fashion, with large amplitude surface deformations stably occurring. The "$L = 8$," $n = 4$, perturbation calculation again led to a phenomenologically similar evolution. The 90° and 45° calculations had the same kinetic energy versus time development. The 22°5 calculation developed with a

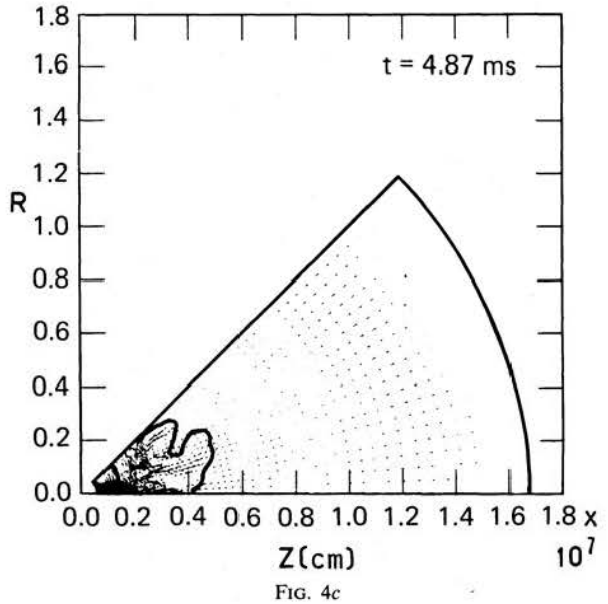


FIG. 4*c*

significantly lower kinetic energy than the other two models. These results indicate "$L = 4$" is preferred in the nonlinear regime of Rayleigh-Taylor instability. This is in keeping with much numerical experience that shows that the largest mode which "just fits" the unstable region is the one which dominates at late times.

We now describe the effect the motion inside 4×10^6 cm has on the outer 17×10^6 cm (region IV). Figure 4*c* shows the entire grid at $t = 4.87$ ms. The "spike and foot" of region III hits the inner core (region I), and the bubble (region II) begins to rise 2.5 ms into the evolution (fig. 4*a*). As it does so, it acts as a piston pushing into region IV. This generates a sound wave which propagates outward. As this sound wave moves down the density gradient (Fig. 2), it steepens into a shock wave (Fig. 4*c*). In addition, the bubble continues to expand at the base of region IV.

Since the details of the equation of state in the outer core are crucial to the correct propagation of the shock (see, e.g., Sack, Bludman, and Lichtenstadt 1980), we do not necessarily believe that the final state of shock found in our simplified two dimensional model is what would actually happen. However, it does seem clear that some type of shock will be generated by the overturn. This shock will run into the standing accretion shock at the outer boundary of region IV, presumably raising the chances of envelope ejection. We will return to this point later.

The last point we wish to discuss in Figure 4 is the rise of the bubble as compressed material from region II expands into its new location. A number of studies have been made on how fast a bubble rises after a nonlinear RT instability (see, e.g., Crowley 1970; Ratafia 1973). The basic result is that a bubble of radius R rises in an acceleration field g at a velocity of

$$V_b = \alpha(Rg)^{1/2} ,$$

© American Astronomical Society • Provided by the NASA Astrophysics Data System

1981ApJ...246..515S

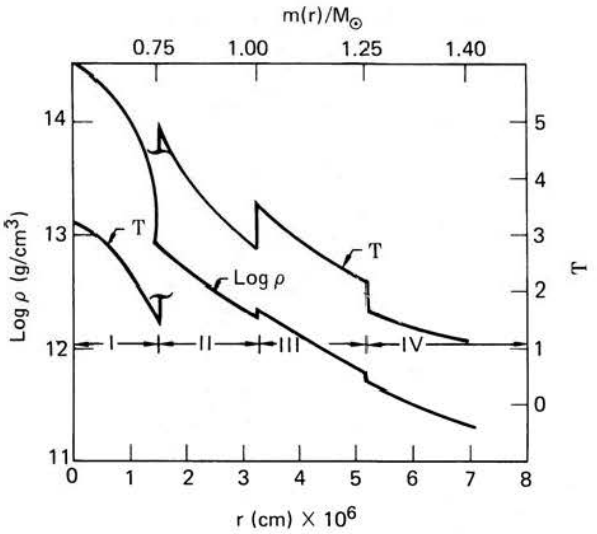


FIG. 5.—Density (g cm^{-3}) and temperature (in arbitrary units) vs. $M(r)/M_\odot$ used in establishing the input for the two dimensional radiation transport plus hydrodynamic model. Also shown are stability regions I–IV.

where α is a dimensionless factor somewhere between

$$0.2 < \alpha < 0.7 .$$

Applied to our present problem with $R \approx 0.1 \times 10^7$ cm, $g \approx 10^{13}$ cm s^{-2}, we would have 7×10^8 cm s^{-1} $< V_b <$ 2.3×10^9 cm s^{-1}. We find that on our 45° run $V_b \approx 10^9$ cm s^{-1}, exactly in the middle of the predicted range. Note that this is much smaller than $V_{\rm sec} = (2GM/r)^{1/2} \approx$ 8×10^9 cm s^{-1} at that radius and thus the bubble will not escape.

c) *Small Density Inversion*

The above three calculations give all the qualitative features we have found to be important in this problem. However, the size of the density inversion used in them (Fig. 2) is excessive given our 1D analysis (Fig. 1). We felt that by overdoing the driving inversion we could set an upper limit to the violence of the turnover. Now we wish to outline briefly the results obtained with the more realistic initial conditions.

Figure 5 and Table 1 give the details of the core model used. Note that there are four pressure scale heights across regions II and III in the initial model. Comparing Figures 5 and 2, one can see that the density inversion is much reduced and that the regions II and III are better zoned (e.g., 18 radial zones in region II versus 8 in the high density inversion run). Another difference is that we used initial velocity perturbations rather than density perturbations. The initial velocity field was taken as:

$$V_r = 0.01 c_S \cos 4\theta , \quad V_\theta = 0 ,$$

at the II/III interface, where c_s is the local sound speed. This velocity was extended into regions II and III, decreasing linearly to zero at the next interface. This change was to test whether our results were sensitive to the initial conditions.

The first model was run with no radiation flow. It was qualitatively very similar to the 45° run (Fig. 4) with high density inversion. The major difference is that it was less energetic and perturbed the inner core only very slightly. There seemed to be no important change caused by the use of velocity perturbations.

We then reran this model with the radiation diffusion on. As explained in § III*a* above, the specific heat was lowered in region III to mimic the lepton depletion. The resulting "temperature" field shown in Figure 5 should be thought of as a combination of thermal temperatures and neutrino chemical potential. An opacity was calculated throughout the core so that the luminosity rose linearly with mass in region I to a value of 4.5×10^{53} ergs s^{-1}. The opacity in the other three regions was chosen so that the luminosity stayed constant at this value. Note that the luminosity represents the luminosity of pair-produced (e, μ, τ) neutrinos which carry heat, but no lepton number. The excess of ν_e neutrinos over antineutrinos caused by electron capture produces a luminosity of roughly a factor of 10 lower in the 1D model. Thus, chemical composition Y_l changes occur over a time scale 10 times longer than this calculation and therefore are ignored in the 2D problem.

The resulting "neutron finger" calculation looks very similar to the no radiation flow case except that the velocities involved are larger. For example, in Figure 6 we show the total kinetic energy (initially due only to the velocity perturbation) which develops during the overturn. The exponentiation phase is clearly shown ($t \lesssim 3$ ms) as well as the nonlinear saturation phase ($t \gtrsim 3$ ms). With the radiation on, this kinetic energy increases (*solid line*) by a factor of ~ 3 at peak, but then reapproaches the nonradiation flow case (*dashed line*). This peak is caused by the initial large drop in heat capacity which forces a strong radial heat flow to try to smooth out the T field. Another measure of the "neutron

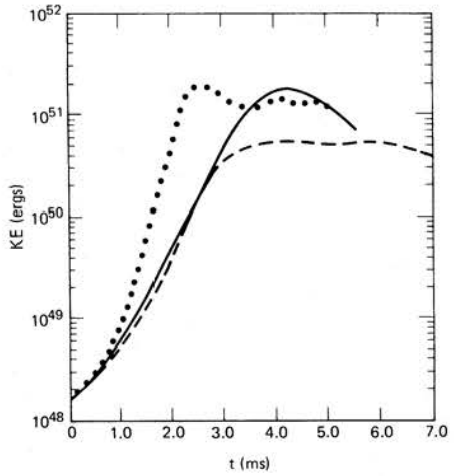


FIG. 6.—Kinetic energy of mass motion resulting from instability for the 45° problem. Kinetic energy for the model with small initial $\Delta\rho$ is given by the dashed curve without heat flow; the solid curve includes heat flow. The dotted curve corresponds to the model with large initial $\Delta\rho$.

© American Astronomical Society • Provided by the NASA Astrophysics Data System

1981ApJ...246..515S

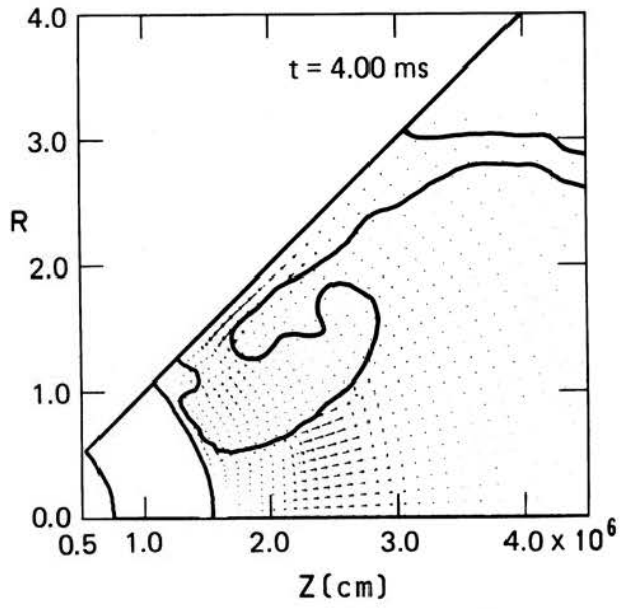


FIG. 7*a*

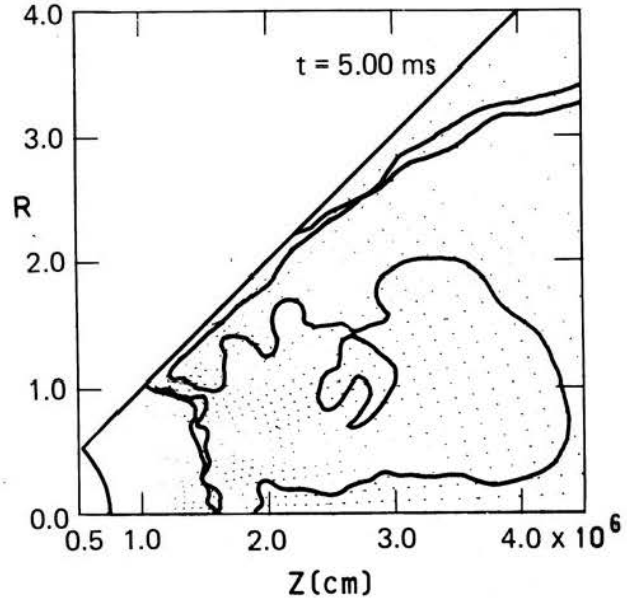


FIG. 7*b*

FIG. 7.—Fluid motion for radiation hydrodynamic model. Initial velocity perturbation of opposite phase relative to Fig. 4. Maximum speed is 4.29×10^9 cm s^{-1} in (*a*) and 6.93×10^9 cm s^{-1} in (*b*). Only inner quarter of mesh is shown.

finger" effect is that the luminosity increases from 4.5×10^{53} ergs s^{-1} to $\sim 6 \times 10^{53}$ ergs s^{-1} due to the added convective flux. Also shown in Figure 6 is the kinetic energy from the large density inversion 45° run. Note that our realistic case of low density inversion produces roughly the same kinetic energy as the high case when one includes the radiation flow. However, the impact of the inner core is much reduced and its surface oscillations are much less violent than in the high density case. Note that in Figure 6 the kinetic energy rises much more rapidly to its peak value for the model with a larger initial $\Delta\rho$.

As a final test of the generality of our conclusions, we ran a radiation diffusion problem with an inital velocity perturbation of opposite phase to all the ones used above. The results were very similar as shown by Figures 7*a* and 7*b*. Figure 7*a* shows the well developed RT–KH "spike and foot" descending along the 45° line instead of along the symmetry axis. At 1 ms later ($t = 5$ ms, Fig. 7*b*) the inversion is complete. Note how small the amplitudes of the induced core oscillations are. As a quantitative measure of the smallness of the vortices induced in region I by the overturn, we point out that the kinetic energy in region I is only 4% of the kinetic energy in region II at $t = 5$ ms Fig. 7*b*), despite its average density being ~ 10 times greater and it contains 0.75 $M_\odot$ versus 0.25 $M_\odot$ in region II. A complete sequence of figures for this calculation has been published in Wilson and Bowers (1980).

A by-product of the calculation is an edit of the quadrupole moment. In the 90° calculation the quadrupole moment Q remains small during the initial 2.5 μs. During the remaining 2.5 μs, corresponding roughly to the observed overturn period $P = 2\pi\omega$, the quadrupole moment can be fitted roughly by $Q(t) = 1.15 \times 10^{45} \sin \omega t$ g cm^2 with $\omega = 2.5 \times 10^3$ s^{-1}. The gravitational radiation intensity is of order $(\dddot{Q})^2 G/45c^5$, so the gravitational energy radiated in a single turnover, $E = (G/45c^5) \int (\dddot{Q})^2 dt$, is about 2.5×10^{46} ergs, or $1.4 \times 10^{-8}\ M_\odot$.

IV. CONCLUSIONS

We conclude that Rayleigh-Taylor overturn does occur in portions of a collapsed core on the time scale of 5–20 ms after bounce discussed by Colgate and Petschek (1979), Bruenn, Buchler, and Livio (1979), and Livio, Buchler, and Colgate (1979). However, we find that the inner core ($0.7\ M_\odot$) is not penetrated by the initial overturn since it is isolated from the outer core by large stabilizing discontinuities. Likewise, we find that the mixing does *not* extend out to the neutrinosphere (much less "significantly beyond") as required by Bruenn, Buchler, and Livio (1979) in their one-dimensional model of this process. The inner portion of the outer core [$0.7\ M_\odot < M(r) < 1.25\ M_\odot$] undergoes a classic Rayleigh-Taylor, Kelvin-Helmholtz nonlinear overturn on a time scale of ~ 5 ms. Heat flow by neutrinos is a significant effect on this time scale. Instead of releasing any of the high-energy inner core neutrinos, the expanding overturned outer core acts as a piston on the very outer core. This creates a shock wave which will reinforce the already existing accretion shock at the core-mantle interface. Whether this new shock will be sufficient to eject the envelope remains to be seen. Furthermore, we caution that the regions of instability depend critically on

© American Astronomical Society • Provided by the NASA Astrophysics Data System

1981ApJ...246..515S

the equation of state, and may change with future refinements (see, e.g., Lattimer and Mazurek 1980).

However, the inversion may have significant effect on the future neutronization of the inner core. Because the depleted lepton material from region III is brought into contact with the highly leptonized material in region I, the microconvection and neutrino flow will be enhanced by the increased gradient in Y_l. Colgate (private communication) has speculated that this will eventually cause the inner core to overturn suddenly, recovering his original effect. Our calculation has established that overturn can occur, but it does not take into consideration future overturns due to further neutronization.

Another effect, emphasized by Colgate (private communication) is that the turbulent eddies sitting over region I may "dig" into region I faster than microdiffusion time scales would predict. To estimate this effect, we use the results in a recent paper of Press (1980). He shows that both experiment and theory predict that a turbulent eddy will erode into a stably stratified fluid with a mixing front rate proportional to $1/\mathscr{R} \cdot \mathscr{R}$ is the Richardson number given by (Press 1980, eq. [4]):

$$\mathscr{R} = g\delta\rho l_0/\rho_0 U_0{}^2 .$$

We find that for late times (i.e., Figs. 4*f* and 7*b*) $\mathscr{R}$ is in the range 50–150 with $U_\rho \sim 2.5 \times 10^9$ cm s^{-1}. Thus the front will advance one eddy scale ($l_0 \sim 10^6$ cm) in $\mathscr{R}$ turnovers of the eddy or 20–60 ms. This is comparable with the diffusion time scale for lepton number. Thus, our calculations would have to be run much longer to see these effects. We point out that since the "eddy digging" relies on a cascade to smaller and smaller length scales (Press 1980), this effect is very difficult to model by finite difference techniques. Only more detailed calculations can decide that issue.

We are grateful for useful conversations with W. D. Arnett, J. Arons, G. Baym, G. Brown, J. R. Buchler, S. A. Colgate, D. Eardley, I. Iben, Jr., J. M. LeBlanc, C. F. McKee, M. L. Norman, D. Pines, S. L. Shapiro, K. S. Thorne, and K. A. Van Riper. This project was started as a result of the workshop on core collapse at the Aspen Center for Physics in 1979. We appreciate the useful comments made by colleagues at the Stellar Collapse Workshop at the Institute of Theoretical Physics, 1980 May. The work was partially supported by the National Science Foundation grant PHY-8001496 and the Department of Energy, under contract W-7405-ENG-48.

REFERENCES

Bruenn, S. W. 1975, *Ann. NY Acad. Sci.*, **262**, 80.
Bruenn, S. W., Buchler, J. R., and Livio, M. 1979, *Ap. J.* (*Letters*), **234**, L183.
Chandrasekhar, S. 1961, *Hydrodynamic and Hydromagnetic Stability* (Oxford: Oxford University Press).
Colgate, S. A., and Petschek, A. G. 1979, *Ap. J.* (*Letters*), **236**, L115.
Colgate, S. A., and White, R. H. 1966, *Ap. J.*, **143**, 626.
Crowley, W. P. 1970, unpublished preprint UCRL-72650.
Daly, B. J. 1967, *Phys. Fluids*, **10**, 297.
Epstein, R. I. 1979, *M.N.R.A.S.*, **188**, 305.
Harlow, F. H., and Welch, J. E. 1966, *Phys. Fluids*, **9**, 842.
Kazanas, D., and Schramm, D. N. 1979, in *Sources of Gravitation Radiation*. ed. L. L. Smarr (Cambridge: Cambridge University Press).
Lamb, D. Q., Lattimer, J. M., Pethick, C. J., and Ravenhall, G. 1978, *Phys. Rev. Letters*, **41**, 1623.
Lamb, H. 1945, *Hydrodynamics* (New York: Dover).
Lattimer, J. M., and Mazurek, T. 1980, preprint.
Livio, M., Buchler, J. R., and Colgate, S. A. 1979, preprint LA-UR-79-3501 (LBC).
Press, W. H. 1980, Center for Astrophysics preprint 1337.
Ratafia, M. 1973, *Phys. Fluids*, **16**, 1207.
Sack, N., Bludman, S. A., and Lichtenstadt, I. 1980, *Phys. Rev. Letters*, **44**, 832.
Spiegel, E. A. 1971, *Ann. Rev. Astr. Ap.*, **9**, 323.
———. 1972, *Ann. Rev. Astr. Ap.*, **10**, 261.
Turner, J. S. 1974, *Ann. Rev. Fluid Mech.*, **6**, 37.
Weaver, T. A., Zimmerman, G. B., and Woosley, S. C. 1978, *Ap. J.*, **225**, 1021.
Wilson, J. R. 1979, in *Sources of Gravitational Radiation*, ed. L. L. Smarr (Cambridge: Cambridge University Press).
Wilson, J. R., and Bowers, R. L. 1980, *Energy Tech. Rev.*, February, p. 17.

ROBERT T. BARTON, RICHARD L. BOWERS, JAMES R. WILSON: Lawrence Livermore Laboratory, L-34, Livermore, CA 94550

LARRY SMARR: Department of Astronomy, University of Illinois, Urbana, IL 61801

© American Astronomical Society • Provided by the NASA Astrophysics Data System